Yb-to-Eu Cooperative Sensitization Upconversion in a Multifunctional Molecular Nonanuclear Lanthanide Cluster in Solution

Sai P. K. Panguluri, Elsa Jourdain, Papri Chakraborty, Svetlana Klyatskaya, Manfred M. Kappes, Aline M. Nonat,* Loïc J. Charbonnière,* and Mario Ruben*

ABSTRACT: Lanthanide metal clusters excel in combining molecular and material chemistry properties. Here, we report an efficient co operative se nsitization UC phenomenon of a Eu^{3+}/Yb^{3+} nonanuclear lanthanide cluster in CD_3OD. The synthesis and characterization of the heteronuclear cluster in the solid state and solution are described together with the UC phenomenon showing E ú$^{3+}$ luminescence in the visible region upon 980 nm NIR excitation of Yb^{3+} at concentrations as low as 100 nM. Alongside being the Eu/Yb cluster to display UC (with a quantum yield value of 4.88×10^{-8} upon 1.13 W cm^{-2} excitation at 980 nm), the cluster exhibits downshifted light emission of Yb^{3+} in the NIR region upon 578 nm visible excitation of Eu^{3+}, which is ascribed to sensitization pathways for Yb through the $^5D_0$ energy levels of Eu^{3+}. Additionally, a faint emission is also observed at *ca.* 500 nm upon 980 nm excitation, originating from the cooperative luminescence of Yb^{3+}. The $[Eu_8Yb(BA)_{16}(OH)_{10}]Cl$ cluster (BA = benzoylacetonate) is also a field-induced s ingle-molecular magnet (SMM) under 4K with a modest U_{eff}/k_B of 8.48 K, thereby joining the coveted list of Yb-SMMs and emerging as a prototype system for next-generation devices, combining luminescence with single-molecular magnetism in a molecular cluster.

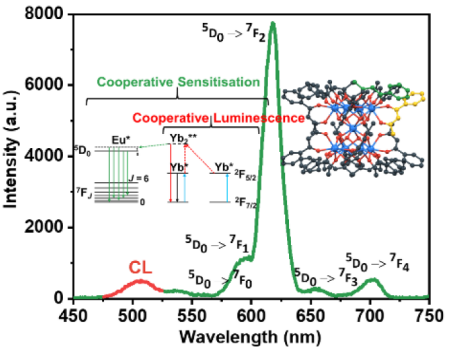

INTRODUCTION

The unique electronic properties of lanthanides have enabled them to play a crucial role in the development of modern technologies. They are routinely employed in LEDs,[1] medical X-ray computed tomography imaging,[2] anticounterfeiting pigments,[3] and strong permanent magnets for diverse applications like MRI scanners and magnetic levitation trains.[4] Additionally, their outstanding optical properties, intricate energy diagrams,[5] and extended lifetimes,[6] drive the development of luminescent tags for bioanalysis[7] and microscopy.[8−10]

In particular, the development of materials[11−14] and molecules[15−17] capable of luminescence upconversion (UC) is booming.[18] UC is the process in which the energy from multiple incoming photons absorbed by a material or a molecule is re-emitted in the form of a single photon of higher energy than the incident light, resulting in an anti-Stokes process. The UC phenomena can be categorized under two broad divisions based on suggestive mechanisms, a classification that has evolved since the pioneering theoretical work of M. Göppert-Mayer and N. Bloembergen in the 1930s−60s.[18a,b] The nonlinear processes, such as two-photon absorption excitation and second harmonic generation (SHG),[18c] fall into one division. These processes are predicted to be weakly efficient as they are based on virtual excited states. The second category of UC processes involves the sequential absorption of individual photons, resulting in improved efficiency (Figure 1). These mechanisms are excited state absorption (ESA), energy transfer UC (ETU), cooperative sensitization (CS), and cooperative luminescence (CL). ESA (Figure 1a) involves the absorption of a photon, leading to an intermediate excited state, subsequently absorbing a second photon to reach the emitting UC luminescent level.[19] In the

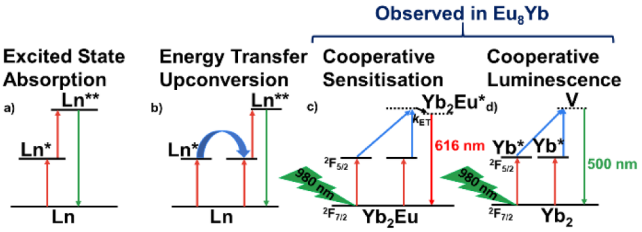

Figure 1. Upconversion mechanisms. a) Excited state absorption. b) Energy transfer upconversion. c) Cooperative sensitization of Eu in Yb_2Eu. d) Cooperative luminescence from Yb_2.

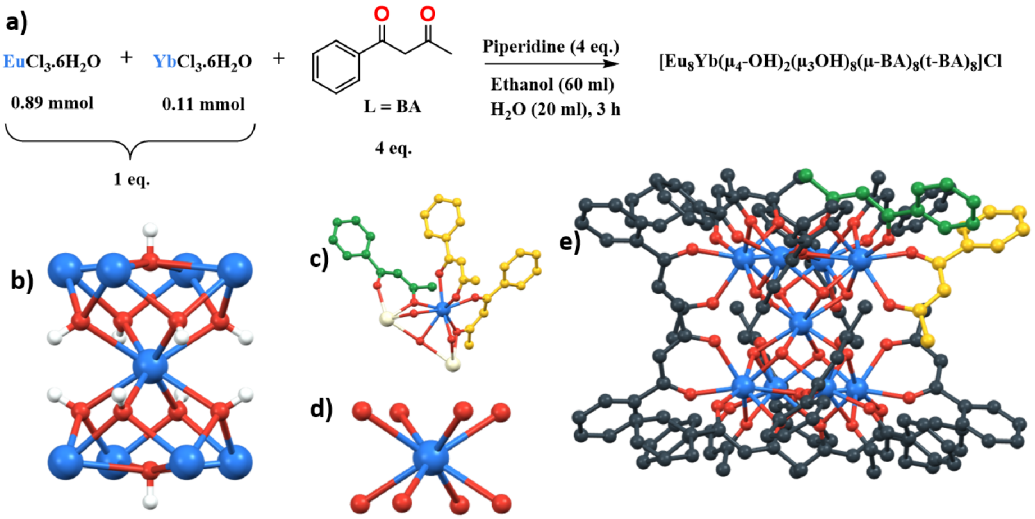

Figure 2. a) Synthetic protocol for preparing the nonanuclear Eu_8Yb complex. B) Single crystal X-ray structure of $[Eu_8Yb(BA)_{16}(OH)_{10}]Cl$, showcasing the arrangement of the nine Ln (blue) and ten hydroxyl groups (O in red and H in white). C) $Ln_{Peripheral}$ coordination sphere: endo ligands (yellow), exo ligands (green), neighboring metal ions (white), oxygens (red). D) $Ln_{Central}$ coordination sphere. E) Single crystal structure of $[Eu_8Yb(BA)_{16}OH_{10}]^+$ ion showcasing BA ligands in gray, with endo and exo BA positions in yellow and green, respectively (hydrogens omitted for clarity).

ETU mechanism reported by François Auzel (Figure 1b)[20,21] the second photon absorption occurs on another ion in the molecule, and an energy transfer occurs between the two ions to feed the emitting upper excited state. CS (Figure 1c) is an interplay between three atoms. Two donor atoms transfer their energy to the third one, which emits light.[22,23] This mechanism is the most frequent in molecular upconverters based on the Tb^{III}/Yb^{III} pair, where the $^5D_4$ excited state of Tb^{3+} around 20600 cm^{-1} is populated through the $Yb^{3+2}F_{5/2}$ excited state at approximately 10200 cm^{-1}.[24−27] Finally, cooperative luminescence (CL) is achieved when the interaction of pairs of lower-energy excited states cooperatively interacts to produce the emission of photons at a higher excited state (Figure 1d). This phenomenon has been reported on solid-state materials[28,29] and more recently using homonuclear Yb^{3+} clusters[26,30] or dimers in solution.[31a] These cooperative processes are treated by two operator transitions between pair levels; they are generally less efficient than ESA or ETU.[31b]

A considerable amount of research has been done on UC, and most of it is based on lanthanide-based solid materials[19−22] or nanoparticles.[32−35] The growing interest in UC materials for biological applications has led to a focus on scaling down UC to the molecular level. This approach aims to enhance solubility, reduce toxicity, improve stability, and create environmentally friendly and reproducible molecular assemblies. The study of molecular-scale UC in solution has gained attention over the past decade, with coordination chemistry playing a central role.[36,37] To observe UC, three prerequisites must be met. First, the elements used for UC emission must have a ladder-like energy level diagram to climb to the higher excited state. This can be achieved by using a single element (e.g., ESA with Er^{3+}[38−40] or by using a pair or combination of elements−donors and acceptors−such as Yb^{III}/Er^{III},[41,42] Yb^{III}/Tb^{III},[24−27] Cr^{III}/Er^{III}[43,44] or Ru^{III}/Yb^{III}[45]) for ETU and CS. The only exception is the cooperative luminescence, which can be observed from the single $Yb^{3+2}F_{5/2}$ excited state of Yb^{3+}.[26,46] In all cases, the intermediate excited states must possess long lifetimes to guarantee an uninterrupted process, leading to the population of the upper state before its return to the ground state through decay. The spatial proximity of energy donors and acceptors[47] is another key to exhibiting energy transfer and, thus, UC. In the past decade, molecular upconversion in solution has been achieved by reducing the de-excitation pathways of Ln(III) complexes, selecting appropriate donor−acceptor pairs, and arranging them spatially. This accomplishment was made possible by designing discrete heteropolynuclear coordination complexes[24,25,39,44,48,49] and molecular clusters.[26,30,31]

More specifically, the authors had previously reported the synthesis of homo- and heterononanuclear Ln^{III} complexes with β-diketonate ligands and, more precisely, acetylacetonate ligands and their deuterated analogs.[26,30] They demonstrated that the obtained clusters are stable in organic solvents, such as methanol. Upconversion studies of the homonuclear Yb_9 cluster $[Yb_9(acac)_{16}(OD)_{10}](OD)$ in CD_3OD revealed the emergence of an emission band at 503 nm when irradiated with 980 nm light, marking the occurrence of molecular CL upconversion in a solution for the first time. Additionally, heterononanuclear complexes containing both Tb^{III} and Yb^{II}, such as $[Tb_xYb_{9-x}(acac)_{16}(OD)_{10}](OD)$, demonstrated CS upconversion, wherein the energy transfer originated from two excited states of Yb^{III} to sensitize Tb^{III}. The deuteration of the ligands as well as the optimization of the donor (Yb^{III}):acceptor (Tb^{III}) ratio allowed for the generation of a highly intense upconversion signal with a UC quantum yield of $\varphi_{UC} = 2.8 \times 10^{-6}$ upon excitation at 980 nm (CD_3OD, p = 2.86 $W.cm^{-2}$).[26,30] Based on these previous studies, we turned toward a mixed Eu^{III}:Yb^{III} nonanuclear $[Eu_8Yb(BA)_{16}OH_{10}]Cl$ cluster with benzoylacetonate (BA) ligands (Figure 2). Here, we present the synthesis of the cluster and its characterization in the solid state and, in solution, its magnetic properties as a Yb-SMM as well as its luminescent properties in the visible (Eu^{III}) and NIR (Yb^{III}) upon excitation in the BA antenna. Last but not least, direct CS upconversion of Eu^{III} is also achieved while Yb is irradiated at 980 nm. Although indirect photosensitization was reported from Tb to Eu,[49a] UC has only been reported once in a recent study for a Eu^{III}:Yb^{III} pair in a molecular complex and in solution through an excited

multimer process.[49b] Isostructural clusters with other lanthanides (Eu, Gd, Tb, Ho, Yb, and Dy) and Y have also been synthesized and examined for comparison.

RESULTS AND DISCUSSION

Synthesis and Crystal Structure. A series of five homonuclear nonanuclear clusters of general composition $[Ln_9(BA)_{16}(OH)_{10}]Cl$ (Ln = Eu, Gd, Tb, Ho, Yb) and three heteronuclear clusters of respective formulas $[Eu_8Yb(BA)_{16}(OH)_{10}]Cl$, $[Dy_8Yb(BA)_{16}(OH)_{10}]Cl$, and $[Y_8Dy(BA)_{16}(OH)_{10}]Cl$ (BA = benzoylacetonate) were synthesized in 59−70% yields using modified procedures from existing literature (Figure 2a).[49c] The synthetic methodology, together with their crystal structures as determined by X-ray crystallography, is presented in Figure 2. Clusters have been characterized by XRD, ESI-TOF mass spectrometry, and elemental analysis (see SI).

The nonanuclear clusters crystallize in a high cubic symmetry packing ($a = b = c = 33.6739(6)$ Å, $\alpha = \beta = \gamma = 90°$, $V = 38183.9$ Å^3, Pn-3n (222)). This closed-packed arrangement results in hexagonal channels (voids) along the body diagonal directions inside the massive unit cell (SI. Section 2.1, Figure 11). The diameter of the channel changes as it runs, with a minimum diameter of approximately 7 Å, not including the van der Waals volume. The channel is spacious enough for solvent molecules and anions (Cl^-) to situate themselves. Within the lattice, the channels stretch along the four-body diagonal directions of the unit cell, causing significant disorder among the smaller components. Even at 120 K, an X-ray analysis cannot resolve this disorder. The solid-state structure of the Ln_9 complexes can be viewed as two pentanuclear square pyramids sharing the apical Ln atom, with a torsion angle of approximately 45° between the two pyramids, resulting in square antiprismatic geometry at the central Ln (Figure 2b). The eight triangular faces of the pyramids are capped by μ_3−OH groups linked to the three Ln atoms at the edges of the triangles, while μ_4−OH bonds connect the four Ln atoms of the two square faces. All Ln atoms except the central one are linked to three β-diketonate ligands through two coordination modes (t-BA in yellow and μ-BA in green, Figure 2c−e). The peripheral Ln ions are coordinated by 16 bidentate BA ligands. Eight of them (shown in yellow, Figure 3e) present an *endo* environment with a bidentate coordination mode to a single metal center (t-BA), while the eight others (shown in green, Figure 2e) are placed in an *exo* environment and coordinate two metal centers in a bridging mode (μ-BA), while being bidentately coordinated to one of the two metals. The coordination sphere of Ln atoms (CN = 8) is completed by hydroxyl ligands: two μ_3−OH hydroxy ligands in the triangular face and two μ_4−OH ligands in the square face. The central lanthanide is octacoordinated with eight μ_3−OH hydroxy ligands (Figure 2b). In the following discussion, these two distinct coordination environments will be termed $Ln_{peripheral}$ and $Ln_{central}$, respectively. Previous studies have shown that such distinct coordination environments can be used to promote site selectivity for heteronuclear lanthanide clusters, with a tendency for the largest ion to occupy the central position.[50] In order to determine if site selectivity was also present in the BA clusters, a set of eight homo- and heterometallic nonanuclear clusters was synthesized and crystallized (SI. Section 2.1. Table 1). Continuous shape measurements (CShMs) were conducted on X-ray crystallographic data within a series, revealing that the

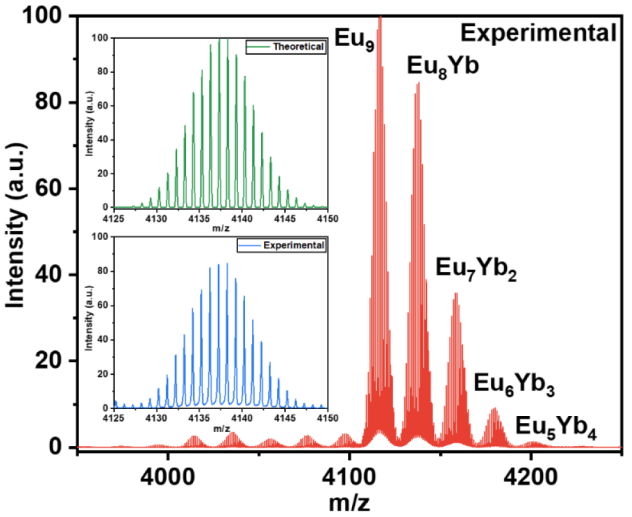

Figure 3. ESI mass spectrum in positive ion mode of the $[Eu_8Yb(BA)_{16}(OH)_{10}]^+$ complex sprayed from a methanol solution. Insets show theoretical (green) and experimental (blue) isotopic patterns of the molecular peak $[Eu_8Yb(BA)_{16}OH_{10}]^+$.

$Ln_{central}$ site exhibits a nearly perfect square antiprismatic geometry with D_{4d} symmetry, while the $Ln_{peripheral}$ site is a biaugmented trigonal prism with C_{2v} symmetry. In addition, the "coordination site cavity" (also called "pocket size") for the two different environments was determined by averaging the Ln-O bond lengths (SI Figures 1−10) for each site.[51] The study demonstrated that the central pocket size is the largest (SI. Section 2.1. Table 1). However, refining the occupancy of each lanthanide site as a superposition of x Ln_1 and $(1-x)$ Ln_2 did not reveal notable site preferences in the cases of Eu/Yb, Dy/Yb, and Y/Dy due to the minimal difference in their ionic radii. The refined values were: $Ln_{Central}$: 96 ± 5% Eu, 4 ± 5% Yb; $Ln_{Peripheral}$: 92 ± 4% Eu, 8 ± 4% Yb.

SEM-EDS analysis gave an atomic composition of 81.3% Eu, 9.6% Yb, and 9.2% Cl, in good agreement with the predicted values of 80% Eu, 10% Yb, and 10% Cl (SI. Section 2.2. Figure 13). The phase purity was also confirmed by measuring the PXRD of fresh crystals taken from the mother liquor (SI. Section 2.3. Figure 14). The crystals that were dried and taken from the vacuum lost the order (SI. Section 2.3. Figure 15). However, a thermal stability study by thermogravimetric analysis (SI. 2.4 Figure 16) confirmed that the compounds remain stable up to 150 °C, and a weight loss of approximately 5% was measured in the temperature range 0−100 °C, which corresponds to the loss of lattice solvent (three EtOH and four H_2O molecules), in perfect agreement with PXRD studies. At temperatures above 210 °C, decomposition of the cluster is observed.

To confirm the homogeneity of the bulk, SEM-EDS analysis was performed on both crystals and powder samples of the Eu_8Yb complex at five different sites, giving an atomic composition of 88.6% Eu and 11.4% Yb, in good agreement with the 88.9% Eu and 11.1% Yb, introduced in the synthesis (SI. Section 2.2. Figure 12). The atomic composition in C and H was also verified by elemental analysis (SI. Section 2.5. Table 2).

ESI-TOF Mass Analysis. Finally, the composition of the cluster in solution was analyzed by electrospray ionization mass spectrometry (ESI-MS). The resulting spectrum (Figure 3.) showed primary peaks at m/z 4116, 4137, and 4158,

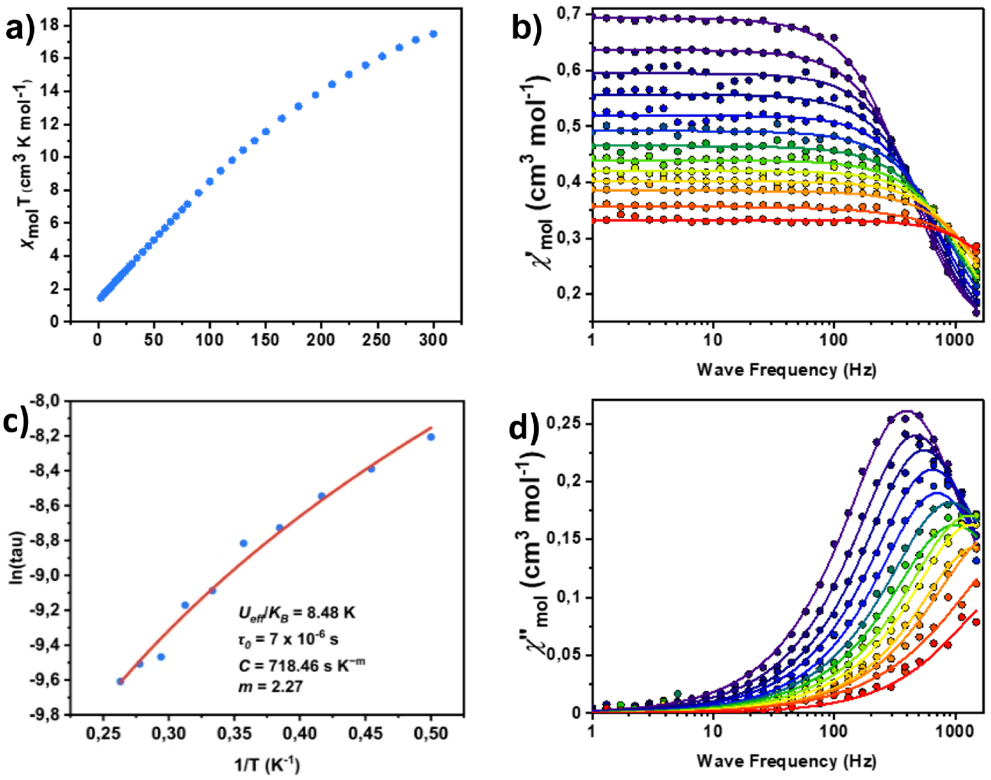

Figure 4. a) Eu_8Yb DC Fit: Temperature product of the molar susceptibility vs. temperature. c) Temperature dependence of the magnetization relaxation times (s), with the solid line representing the best fit using eq 2 (red line: Raman contribution); (b,d) in-phase and out-of-phase susceptibilities vs. frequency fits of Eu_8Yb under a 1750 Oe applied dc field (Debye model).

corresponding to the monocharged Eu_9, Eu_8Yb, and Eu_7Yb_2 complexes, respectively. The other peaks on the higher m/z side with intensity <10% of the most abundant Eu_9 peak are due to complexes with higher Yb replacing Eu in the metal core (Eu_6Yb_3, Eu_5Yb_4). The full range ESI MS spectrum is presented in the Supporting Information (SI. Section 2.6. Figure 17). The relative integrals of the isotopic patterns were used to calculate the proportion (P_i) of the Ln^1 and Ln^2 species at mole fraction x of Ln^1. Experimental values ($P_{0,exp}$ = 0.41 for [Eu_9]; $P_{1,exp}$ = 0.37 for [$YbEu_8$]; $P_{2,exp}$ = 0.17 for [Yb_2Eu_7]; $P_{3,exp}$ = 0.05 for [Yb_3Eu_6]; and $P_{4,exp}$ = 0.008) demonstrate an overall good agreement with the perfect statistic distribution as obtained by eq 2), under the hypothesis that all coordination sites in the clusters are chemically equivalent and all Ln(III) clusters have similar ionization abilities:

$$P_i = \frac{n!}{i!(n-1)!} * x^i(1-x)^{n-i} \quad (2)$$

where n represents the total number of sites, i.e., Nine in a nonanuclear complex; i represents the number of Ln^1 ions (here Yb); x= 1/9; $P_{0,th}$ = 0.346 for [Eu_9]; $P_{1,th}$ = 0.389 for [$YbEu_8$]; $P_{2,th}$ = 0.195 for [Yb_2Eu_7]; $P_{3,th}$ = 0.057 for [Yb_3Eu_6]; and $P_{4,th}$ = 0.011).

Complexes with a higher molar fraction of Yb have a probability lower than 1%. This analysis also shows that for a Yb:Eu stoichiometric ratio of 1:8, complexes containing at least two Yb atoms represent more than 22% of all possible nonanuclear complexes formed, which is favorable to the observation of molecular upconversion with a CS mechanism (see below).

Magnetic Measurements. Trivalent lanthanide ions possess strong spin−orbit coupling, resulting in their highly anisotropic nature. This feature has led to the emergence of various coordination compounds of Ln(III) exhibiting SMM behavior.[52] The increasing popularity of single-molecule magnetism in recent years is due to the potential use of SMMs in various quantum technological fields. The vast majority of Ln^{3+} complexes featuring photoluminescence and SMM behavior are based on Dy^{3+}, closely followed by Yb^{3+} complexes. SMMs based on Yb would require a strong axial magnetic anisotropy and, with appropriate system designs, can reach energy barriers of magnetization reversal as high as 45 cm^{-1}.[53] Furthermore, Yb complexes emitting in the Near Infrared (NIR) region are particularly intriguing due to their potential for combining magnetic properties with luminescence, offering prospects for advanced information storage and quantum computing applications.[54] To the best of our knowledge, no compounds exhibiting both upconversion (UC) luminescence and field-induced SMM behavior have ever been reported. In this study, we analyzed the dc magnetic behavior of Eu_8Yb (using a weighted average of all the clusters as MW found in the Mass spectrum (SI. Section 2.7)) under a 1000 Oe magnetic field in the temperature range of 2−300 K. Figure 4a shows the corresponding $\chi_m T$ vs. T dependencies. As the temperature decreases from 300 to 2K, there is a consistent decrease in $\chi_m T$ for all nonisotropic lanthanide-containing complexes. This can be attributed to the depopulation of the m_j levels split by the crystal field and the weak antiferromagnetic intermolecular interactions between the Ln^{3+} ions. The dependencies of $\chi_m T$ vs. T, especially the low value at low T, indicate the incorporated Eu^{3+} ion's absence of thermally populated excited states and highlight their decisive effect on

the dc magnetic behavior. Therefore, the sole contributor of $\chi_m T$ at 2 K is Yb^{3+}, which explains the very low value, as Eu^{3+} has no contribution at such low temperatures. In contrast, at 300 K, the $\chi_m T$ value is 17.47 cm^3 K mol^{-1}, and the calculated value is eight times 1.7 (Eu^{3+}) and 2.57 (Yb^{3+}) = 16.14 cm^3 K mol^{-1} for nine noninteracting ions. The small discrepancy is within the acceptable range of a 10% error. Since Yb^{3+} has a prolate electron density and, therefore, is anisotropic, we investigated the magnetization dynamics by ac susceptibility measurements on the same sample under an applied dc field of 1750 Oe, in order to establish whether the properties of the single-molecule magnets (SMMs) are exhibited (Figure 4b–d). The slow relaxation magnetic behavior, which may originate from the significant separation between the ground and the first excited states, was investigated. No out-of-phase signal was observed at zero dc field, likely due to quantum tunneling of the magnetization (QTM), which is enabled by the mixture of the m_J levels in the ground state. However, a clear out-of-phase signal was observed upon application of a small dc field. Under a static dc field of 1750 Oe, the signal of the ac magnetic susceptibility was optimized in the frequency range of 1 to 1500 Hz, where an out-of-phase signal was observed up to 5.6 K (Figure 4d). These data were fit to a generalized Debye model, from which a distribution (α) of relaxation times (τ) can be extracted. Further insights into the magnetic relaxation processes of the complex were achieved by evaluating the $\ln(\tau^{-1})$ vs. T plot (Figure 4c). Considerable deviation from the linear course of the dependencies evidence the occurrence of the relaxation mechanisms additional or different from the Orbach one. Hence, the fit by other mechanisms and/or their sums were performed.

$$\tau^{-1} = \underbrace{\tau_0^{-1}\exp\left(-U_{\text{eff}}/k_B T\right)}_{\text{Orbach}} \underbrace{+CT^m}_{\text{Raman}} \underbrace{+\tau_{\text{QTM}}^{-1}}_{\text{QTM}} \qquad (3)$$

The fittings by the sets of mechanisms other than the Raman fit were unsatisfactory and led to overparameterization. As a consequence, we approximated the relaxation data in the entire temperature range by the Raman relaxation mechanism ($\tau_{\text{Raman}}^{-1} = C_{\text{Raman}} \cdot T^m$–Raman). We also fitted the data with an additional Orbach contribution owing to the linearity of the data points (deviation from exponential behavior) at temperatures above 3 K to determine the effective energy barrier and the relaxation time. The resulting best-fit parameters are τ_0 = 4.4×10^{-6} s, U_{eff}/k_B = 8.48 K, C = 718.46 s^{-1} K^{-2},[27] and m = 2.27. These parameters indicate that the $YbEu_8$ cluster exhibits SMM behavior, characterized by a relatively short relaxation time and a moderate energy barrier, especially when compared to other SMMs based on Yb^{III} reported in the literature.[55] This is, to the best of our knowledge, the first example of a Yb^{III}-based SMM that also possesses upconversion properties (as illustrated below). Throughout the temperature range (2–4 K), the exponentially increasing τ^{-1} values plotted on a logarithmic scale confirm the presence of a Raman relaxation process. Finally, at high temperatures, deviation from this exponential behavior might suggest the onset of an Orbach relaxation mechanism, which has been observed in a limited number of Yb^{III}-based complexes.[53,56,57] The combination of luminescence (see below) and magnetic properties has also attracted interest due to the possible correlation between the electronic structure of complexes extracted from optical properties and the effective energy barriers determined by dynamic magnetic measurements.[58] Furthermore, beyond just understanding the SMM behavior, light can be used as a noninvasive trigger to manipulate the spin state of a system, while optical measurements can act as probes to study the environment of discrete molecules.[59]

Photophysical Studies. The photophysical properties of the $[Eu_8Yb(BA)_{16}(OH)_{10}]Cl$ cluster have been studied at room temperature in CD_3OD solutions. Its UV–vis-NIR absorption spectrum (Figure 5) displays a broad band in the

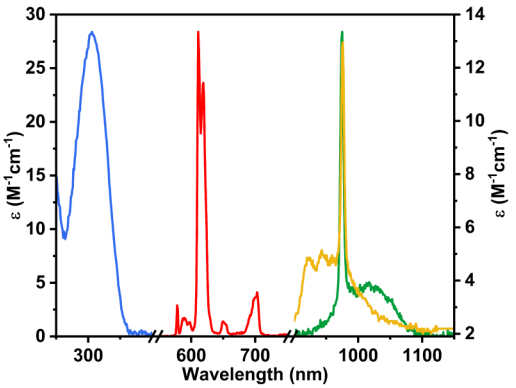

Figure 5. UV–vis and NIR absorption spectra (blue (45 μM) and yellow (1 mM), respectively) and normalized emission spectra (λ_{exc} = 326 nm) in the visible (red: Eu, 45 μM, 399 nm Filter) and NIR (green: Yb, 45 μM, 800 nm Filter) domains for the Eu_8Yb cluster in CD_3OD.

UV region with a maximum at 306 nm (ε = 28.4×10^4 $M^{-1}cm^{-1}$), attributed to transitions centered on the BA ligands, and a broad absorption band centered at 976 nm (ε = 12.95 $M^{-1}cm^{-1}$ in CD_3OD), which is attributed to the $^2F_{5/2} \leftarrow {}^2F_{7/2}$ transition of Yb^{III}.

Upon excitation into the BA absorption band (326 nm), the cluster displays two sets of emission bands (Figure 5.). Those in the visible region correspond to the $^5D_0 \rightarrow {}^7F_J$ (J = 0 to 4) transitions of Eu (Φ_{Eu} = 0.13% in CD_3OD), and the broad emission band peaking at 974 nm corresponds to the $^2F_{5/2} \rightarrow {}^2F_{7/2}$ transition of Yb (Φ_{Yb} = 0.26% in CD_3OD). The corresponding luminescence lifetime of Yb in CD_3OD was 13.9 ± 0.1 μs at 974 nm. Lifetime and quantum yield values are similar to those reported for the Tb_1Yb_8 cluster with acac antennae.[30] According to the formalism of Werts and coworkers,[60] the radiative lifetime was estimated from the integral of the Yb absorption spectrum (SI. Section 2.2. Figure 30) to amount to 810 μs, which is in line with literature data on other Yb clusters.[30] With these values, the intrinsic quantum yield of Yb was calculated to be 1.7%, and the sensitization efficiency amounted to 16%, a result similar to the previously obtained value of 22% for unsubstituted acac-d7 ligands.[26]

Time-dependent luminescence decay profiles were also measured for the Eu^{III} emission (λ_{exc} = 326 nm) and fitted to biexponential curves with the corresponding lifetimes: τ_1= 0.196 ± 0.001 ms (B_1 = 85%), τ_2= 1.265 ± 0.002 ms (B_2 = 15%) measured at 578 nm, and τ_1= 0.189 ± 0.001 ms (B_1 = 84%), τ_2= 1.256 ± 0.002 ms (B_2 = 16%) at 612 nm, respectively. Both fits are in very good agreement and reflect the presence of the Eu^{III} ions in two distinct chemical environments: the peripheral site (τ_1), with a major contribution due to the direct photosensitization from the BA antennae, and the central site (τ_2), present in a smaller

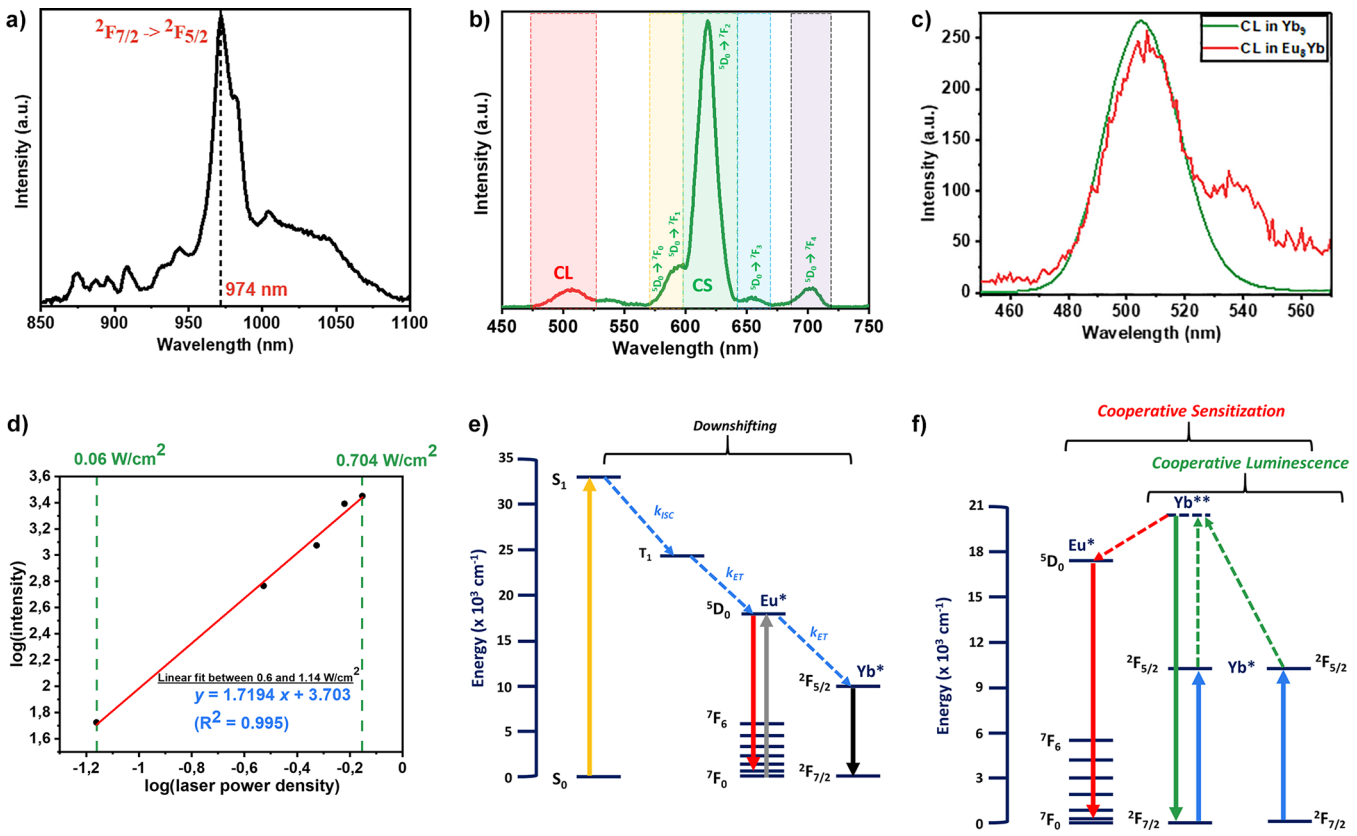

Figure 6. a) Downshifted PL emission of the Eu_8Yb complex ([c] = 0.5 mM, CD_3OD, and λ_{exc} = 578 nm). b) UC emission of the Eu_8Yb complex ([c] = 45 μM, CD_3OD, λ_{exc} = 980 nm, and p = 2.86 W cm^{-2}). c) Cooperative luminescence (CL) emission of the Yb_9 complex (Green, [c] = 2.04 mM, CD_3OD, λ_{exc} = 980 nm, p = 10.8 W cm^{-2}) vs. CL emission of the Eu_8Yb complex (Red, [c] = 45 μM, CD_3OD, λ_{exc} = 980 nm, p = 10.8 W cm^{-2}), normalized according to the concentration of Yb^{3+} in the sample. d) UC intensity as a function of the incident pump power density on a log/log scale. e) Schematic representation of the absorption (yellow) and downshifting (black). f) Schematic representation of the cooperative luminescence (green) and the cooperative sensitization (red) processess.

proportion but exhibiting a longer lifetime due to enhanced protection against nonradiative quenching by solvent molecules.[61] Overall, the Eu^{III} emission quantum yield was measured to be Φ_{Eu} = 0.13% in CD_3OD (λ_{exc} = 326 nm). The radiative lifetime of Eu was also estimated using the formalism of Werts et al.[60] and was found to be 1.32 ms, in relatively good agreement with the value found for Yb, considering the uncertainties inherent in the method. Noteworthy, these values are significantly smaller than common values observed for Eu complexes with β-diketonate ligands.[62]

The relatively low quantum yield of Eu suggests either inefficient sensitization by the BA ligands or the occurrence of nonradiative quenching processes due to vibrations, concentration quenching,[63] or energy transfer to the Yb$^2F_{5/2}$ excited state. Quantification of the Eu → Yb energy transfer was achieved by measuring the Eu luminescence lifetimes of the Eu_9 cluster. The corresponding values are τ_1= 0.253 ± 0.001 ms (B_1 = 81.40%) and τ_2= 1.484 ± 0.002 ms (B_2 = 18.6%) for the 578 nm emission peak, and τ_1 = 0.256 ± 0.001 ms (B_1 = 79.5%) and τ_2 = 1.586 ± 0.002 ms (B_2 = 20.5%) at 612 nm. A decrease of approximately 24% in the τ_1 lifetime of Eu, as well as a 15% shortening of τ_2, were observed following the incorporation of Eu into the Yb_9 structure. This decrease in the average lifetime amounts to 18% and is ascribed to the energy transfer from Eu to Yb within Eu_8Yb. Consequently, the efficiency of this energy transfer was estimated to be 18%. In addition, a radiative lifetime of 1.65 ms was determined for this cluster, consistent with other values measured within this study.

In the same cluster, Stokes downshifted photoluminescence of Yb in the NIR was also observed when exciting in the visible absorption band of Eu at 578 nm ($^5D_0$ → $^7F_0$) in CD_3OD (Figure 6a). The characteristic $^2F_{5/2}$ → $^2F_{7/2}$ Yb emission is observed, indicating that Yb sensitization occurs as a result of the energy transfer from the $^5D_0$ energy levels of Eu to the $^2F_{5/2}$ excited state of Yb. Based on this intermetallic communication, we thus focused on the reverse mechanism, namely the cooperative sensitization of Eu by Yb.

In the same manner as the downshifting measurements, upconversion experiments were carried out at room temperature in CD_3OD solutions. When the Eu_8Yb cluster was excited in the NIR$^2F_{5/2}$ ← $^2F_{7/2}$ absorption band of Yb at 980 nm, a striking feature was observed in the spectrum: a strong emission in the visible region that had the typical spectral signature of the Eu emission with maxima at 612 nm and the five $^5D_0$ → ^7F_J (J = 0–4) transitions (Figure 6b). Additionally, a small peak at 505 nm was also present, which was assigned to the cooperative luminescence between two Yb centers (Figure 6b), as previously observed in homonuclear Yb_9 clusters.[26,30] Looking closely (Figure 6c, **red curve**), a weak and broad emission band was also noticed at 535–540 nm, which was attributed to the contribution of the $^5D_1$ → $^7F_0$ emission, which is often observed in Eu β-diketonate complexes.[64] This observation is a strong argument to propose that cooperative

sensitization occurs from the doubly excited state of Yb to the $^5D_1$ level of Eu, with a subsequent population of the $^5D_0$ state.

The CL intensity from Eu_8Yb and Yb_9 was also compared (Figure 6c) in order to gain insights into the influence of the Yb doping ratios on CL efficiency. Although a weak signal is measured from Eu_8Yb in comparison to Yb_9, this difference could mainly be ascribed to the variations in the Yb^{3+} concentrations (9 μM and 18.4 mM, respectively) of the two samples. In addition, it should be noted that, theoretically, CL can occur in clusters with a Yb:Eu 1:8 composition owing to the statistical presence of clusters containing two or more Yb centers (22%, as explained above). Taking into account the smaller concentration of the Eu_8Yb sample in comparison to the Yb_9 cluster and the fact that only 22% of molecules are capable of CL, Figure 6d suggests that CL might be more efficient in Eu_8Yb than in Yb_9, which could be explained by the reduction of concentration quenching.

To further confirm the upconversion luminescence mechanisms, the overall upconversion luminescent intensity (CS + CL) was recorded as a function of the incident pump power density, and the logarithmic representation presents a quasi-linear profile with slopes of 1.7 for CS at 612 nm and 1.6 for CL at 505 nm, respectively (Figure 6d and SI. Section 2.8. Figure 31). The quadratic dependence provides evidence for the absorption of two photons by the Yb metal centers, in accordance with the upconversion mechanism.[48,65]

The proposed mechanism in a prototype complex, such as $Eu_{9-x}Yb_x$ (where $x > 1$), entails a major contribution of CS and a minor contribution of CL of Yb (Figure 7). As previously

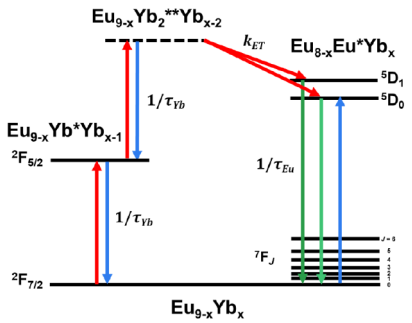

Figure 7. Schematic representation of the proposed cooperative photosensitization process (UC mechanism).

described, CS involves a first absorption of the photon by one Yb atom, leading to an $[Eu_{9-x}Yb^*Yb_{x-1}]$ excited species, followed by the absorption of a second photon by a neighboring Yb ion, hence, forming the $[Yb_2^{**}Eu_{9-x}Yb_{x-2}]$ intermediate, which transfers its energy to $^5D_1$ and $^5D_0$ levels of Eu, creating the $[Eu_{8-x}Eu^*Yb_x]$ excited states, which then decays to the ground state by emission of visible light. As for CL, two photon absorption by two Yb ions in the same cluster results in a doubly Yb_2^{**} excited state, which decays in the visible, showing a transition at 505 nm. As expected, a $[Eu_9(BA)_{16}(OH)_{10}]Cl$ cluster without any Yb did not show any upconversion luminescence in the visible region when irradiated at 980 nm (SI. Section 2.8, Figure 32).

Using established procedures,[25] we calculated the UC quantum yield (Φ_{UC}) of the $YbEu_8$ cluster in CD_3OD solution at room temperature, resulting in a value of 4.84×10^{-8} upon exciting at 980 nm (1.13 W cm^{-2}). This value is in line with the previous data reported for UC quantum yields. It is 6 to 25 times larger when compared to the best UC Er complexes ($1.95 \times 10^{-9} < \Phi_{UC} < 8 \times 10^{-9}$ at p = 21 W cm^{-2}),[48] and 3 times larger than the first heteropolynuclear Yb/Tb UC complexes (1.4×10^{-8} at p = 10.3 W cm^{-2}). Nevertheless, this value is not as high as the quantum yields recently reported for Yb:Tb clusters,[26,30] which could be correlated to the increased propensity of Eu to be quenched by nonradiative deactivations. Another possible explanation for this reduced UC efficiency may be found in the lower spectral overlap of the CL emission of Yb** with the $^5D_1$ absorption band of Eu around 535 nm, compared to that of the $^5D_4$ absorption band of Tb at 485 nm. In conclusion, our findings highlight the role of supramolecular clusters in achieving efficient upconversion in solution by providing a scaffold capable of incorporating a unique lanthanide (Yb for CL) and/or donor/acceptor pairs (for CS) with appropriate Ln−Ln distances and a tunable statistical distribution. Additionally, we provide evidence of the potential to achieve cooperative sensitization (CS) upconversion and downshifting in a molecular cluster containing Eu and Yb.

EXPERIMENTAL SECTION

Preparation of $[Ln_nLn'_{9-n}(BA)_{16}(OH)_{10}]Cl$. Benzoylacetone (BA) (649 mg, 4 mmol, 4 equiv) and piperidine (396 mL, 4 mmol, 4 equiv) were dissolved in C_2H_5OH (60 mL). The mixture was heated while stirring at 75 °C for 1 h. Meanwhile, $LnCl_3.6H_2O$ (x mmol, n/9 equiv.) and $Ln'Cl_3.6H_2O$ (1−x mmol, (9−n)/9 equiv.) were dissolved in 20 mL of H_2O and added dropwise to the alcoholic solution, and the reaction mixture was stirred at 75 °C for 3 h until obtaining a transparent solution. After three h, the heating was turned off, and the solution cooled down to room temperature, filtered out, and left undisturbed to obtain crystals. After 1 week, we could harvest cubic-shaped crystals ideal for X-ray analysis. Details and characterization by XRD, ESI-TOF mass spectrometry, and elemental analysis are provided in the Supporting Information.

CONCLUSION

By doping Yb ions into Europium nonanuclear complexes, we were able to create a first-ever multifunctional heteronuclear $[Eu_8Yb(BA)_{16}(OH)_{10}]Cl$ complex that displays highly efficient cooperative UC luminescence in solution based on the Yb/Eu donor/acceptor pair and rare single-molecule magnet (SMM) behavior characterized by a slow relaxation of magnetization. The UC process is among the most efficient molecular or supramolecular UC probes reported to date[25,43,48] and can be observed in solution at concentrations as low as 100 nM. Furthermore, this marks a rare instance of direct cooperative sensitization (CS) upconversion within a molecular cluster that incorporates both Eu and Yb. By utilizing readily accessible β-diketonate ligands along with a diverse range of Ln donor−acceptor dyads and structures, we anticipate achieving even more efficient upconversion (UC) systems. In addition to the attractivity of UC systems for bioanalytical applications,[66] we believe that the development of UC luminescent Ln-SMMs is a promising field of research with many corners still unexplored. The incorporation of multiple functionalities into a single molecule can potentially enhance our understanding of SMM behavior, especially considering that SMMs are intended for implementation in next-generation nanocircuits for quantum computation.[67]

Accession Codes

CCDC 2016566−2016567, 2017536, 2288023, and 2331085 contain the supplementary crystallographic data for this paper. These data can be obtained free of charge via www.ccdc.cam.ac.uk/data_request/cif, or by emailing data_request@ccdc.cam.ac.uk, or by contacting The Cambridge Crystallographic Data Centre, 12 Union Road, Cambridge CB2 1EZ, UK; fax: +44 1223 336 033.

AUTHOR INFORMATION

Corresponding Authors

Aline M. Nonat − *Equipe de Synthèse pour l'Analyse (SynPA), Institut Pluridisciplinaire Hubert Curien (IPHC), UMR 7178, CNRS/Université de Strasbourg, ECPM, Strasbourg 67087, France;* orcid.org/0000-0003-0478-5039; Email: aline.nonat@unistra.fr

Loïc J. Charbonnière − *Equipe de Synthèse pour l'Analyse (SynPA), Institut Pluridisciplinaire Hubert Curien (IPHC), UMR 7178, CNRS/Université de Strasbourg, ECPM, Strasbourg 67087, France;* orcid.org/0000-0003-0328-9842; Email: l.charbonn@unistra.fr

Mario Ruben − *Institute of Quantum Materials and Technologies (IQMT), Karlsruhe Institute of Technology, Karlsruhe 76311, Germany; Institute of Nanotechnology, Karlsruhe Institute of Technology (KIT), Karlsruhe 76311, Germany; Centre Européen de Sciences Quantiques, Institut de Science et d'Ingénierie Supramoléculaires (ISIS, UMR 7006), CNRS-Université de Strasbourg, Strasbourg, Cedex 67083, France*; Email: mario.ruben@kit.edu

Authors

Sai P. K. Panguluri − *Institute of Quantum Materials and Technologies (IQMT), Karlsruhe Institute of Technology, Karlsruhe 76311, Germany;* orcid.org/0000-0003-0676-5381

Elsa Jourdain − *Equipe de Synthèse pour l'Analyse (SynPA), Institut Pluridisciplinaire Hubert Curien (IPHC), UMR 7178, CNRS/Université de Strasbourg, ECPM, Strasbourg 67087, France*

Papri Chakraborty − *Institute of Nanotechnology, Karlsruhe Institute of Technology (KIT), Karlsruhe 76311, Germany;* orcid.org/0000-0002-1353-7734

Svetlana Klyatskaya − *Institute of Nanotechnology, Karlsruhe Institute of Technology (KIT), Karlsruhe 76311, Germany;* orcid.org/0000-0003-2883-750X

Manfred M. Kappes − *Institute of Nanotechnology, Karlsruhe Institute of Technology (KIT), Karlsruhe 76311, Germany;* orcid.org/0000-0002-1199-1730

Funding

E uropean Union's Framework Programme for Research and Innovation, Horizon 2020, under the Marie Sklodowska-Curie Grant Agreement No. 847471 (QUSTEC).

Notes

The authors declare no competing financial interest.

ACKNOWLEDGMENTS

S.P.K.P. acknowledges late. Dr. Andreas Eichhöfer, Dr. Christopher E. Anson, Dr. Asato Mizuno, Dr. Olaf Fuhr, and Prof. Dieter Fenske for their assistance in PXRD and SC-XRD measurements.

REFERENCES

(1) Shimizu, Y.; Sakano, K.; Y, N.; Moriguchi, T. *Light Emitting Device With Blue Light Led And Phosphor Components* US 72,15,074 B2, 2007.

(2) Siemens Medical Solutions USA, IncGhelmansarai, F. A. *X-ray Scintillator Compositions For X-ray Imaging Applications*, US 6,630,675 B2, 2001.

(3) Emsley, J.; *Europium* https://eic.rsc.org/elements/europium/2020007. (accessed 08 October 2019).

(4) Sagawa, M.; Mizoguchi, T. *Sintered Neodymium Magnet and manufacturing method therefor Abstract*. Intermetallics Co. Ltd [JP], EP 2,696,355 A1, 2014.

(5) Bünzli, J.-C. G. Lanthanide Luminescence for Biomedical Analyses and Imaging. *Chem. Rev.* **2010**, *110* (5), 2729−2755.

(6) Eliseeva, S. V.; Bünzli, J.-C. G. Lanthanide luminescence for functional materials and bio-sciences. *Chem. Soc. Rev.* **2010**, *39* (1), 189−227.

(7) Li, J.; Zhu, Y.; Xu, H.; Zheng, T.-F.; Liu, S.-J.; Wu, Y.; Chen, J.-L.; Chen, Y.-Q.; Wen, H.-R. A Benzothiadiazole-Based Eu3+ Metal−Organic Framework as the Turn-On Luminescent Sensor toward Al^{3+} and Ga^{3+} with Potential Bioimaging Application. *Inorg. Chem.* **2022**, *61* (8), 3607−3615.

(8) Liu, Y.; Lu, Y.; Yang, X.; Zheng, X.; Wen, S.; Wang, F.; Vidal, X.; Zhao, J.; Liu, D.; Zhou, Z.; et al.et al. Amplified stimulated emission in upconversion nanoparticles for super-resolution nanoscopy. *Nature* **2017**, *543* (7644), 229−233.

(9) Hamon, N.; Bridou, L.; Roux, M.; Maury, O.; Tripier, R.; Beyler, M. Design of Bifunctional Pyclen-Based Lanthanide Luminescent Bioprobes for Targeted Two-Photon Imaging. *J. Org. Chem.* **2023**, *88* (13), 8286−8299.

(10) Park, Y. I.; Lee, K. T.; Suh, Y. D.; Hyeon, T. Upconverting nanoparticles: a versatile platform for wide-field two-photon microscopy and multi-modal in vivo imaging. *Chem. Soc. Rev.* **2015**, *44* (6), 1302−1317.

(11) Chen, B.; Wang, F. Combating concentration quenching in upconversion nanoparticles. *Acc. Chem. Res.* **2020**, *53* (2), 358−367.

(12) Bharmoria, P.; Bildirir, H.; Moth-Poulsen, K. Triplet−triplet annihilation based near infrared to visible molecular photon upconversion. *Chem. Soc. Rev.* **2020**, *49* (18), 6529−6554.

(13) Richards, B. S.; Hudry, D.; Busko, D.; Turshatov, A.; Howard, I. A. Photon upconversion for photovoltaics and photocatalysis: a critical review: focus review. *Chem. Rev.* **2021**, *121* (15), 9165−9195.

(14) Liu, S.; Yan, L.; Huang, J.; Zhang, Q.; Zhou, B. Controlling upconversion in emerging multilayer core−shell nanostructures: from fundamentals to frontier applications. *Chem. Soc. Rev.* **2022**, *51* (5), 1729−1765.

(15) Yin, H.-J.; Xiao, Z.-G.; Feng, Y.; Yao, C.-J. Recent Progress in Photonic Upconversion Materials for Organic Lanthanide Complexes. *Materials* **2023**, *16* (16), 5642.

(16) Nonat, A. M.; Charbonnière, L. J. Upconversion of light with molecular and supramolecular lanthanide complexes. *Coord. Chem. Rev.* **2020**, *409*, 213192.

(17) Bolvin, H.; Furstenberg, A.; Golesorkhi, B.; Nozary, H.; Taarit, I.; Piguet, C. Metal-based linear light upconversion implemented in molecular complexes: challenges and perspectives. *Acc. Chem. Res.* **2022**, *55* (3), 442−456.

(18) (a) Göppert-Mayer, M. Über Elementarakte mit zwei Quantensprüngen. *Ann. Phys.* **1931**, *401*, 273−294. (b) Bloemberger, N. Solid State Infrared Quantum Counters. *Phys. Rev. Lett.* **1959**, *2*, 84. (c) Auzel, F. Upconversion and Anti-Stokes Processes with f and d Ions in Solids. *Chem. Rev.* **2004**, *104* (1), 139−174.

(19) Porter, J. F. Fluorescence Excitation by the Absorption of Two Consecutive Photons. *Phys. Rev. Lett.* **1961**, *7* (11), 414−415.
(20) Auzel, F. Compteur quantique par transfert denergie de Yb^{3+} a Tm^{3+} dans un tungstate mixte et dans un verre germanate. *Comptes Rendus Hebd. Des Seances L Acad. Des Sci. Ser. B* **1966**, *263* (14), 819.
(21) Auzel, F. Compteur quantique par transfert d'energie entre deux ions de terres rares dans un tungstate mixte et dans un verre. *C. R. Acad. Sci. Paris* **1966**, *262*, 1016−1019.
(22) Salley, G. M.; Valiente, R.; Guedel, H. U. Luminescence upconversion mechanisms in Yb^{3+}−Tb^{3+} systems. *J. Lumin.* **2001**, *94*−*95*, 305−309.
(23) Livanova, L.; Saitkulov, I.; Stolov, A. Summation processes for quanta in CaF_2 and SrF_2 single crystals activated with Tb^{3+} and Yb^{3+} ions. *Sov. Phys. Solid State* **1969**, *11*, 750.
(24) Souri, N.; Tian, P.; Platas-Iglesias, C.; Wong, K.-L.; Nonat, A.; Charbonnière, L. J. Upconverted photosensitization of Tb visible emission by NIR Yb excitation in discrete supramolecular heteropolynuclear complexes. *J. Am. Chem. Soc.* **2017**, *139* (4), 1456−1459.
(25) Nonat, A.; Bahamyirou, S.; Lecointre, A.; Przybilla, F.; Mely, Y.; Platas-Iglesias, C.; Camerel, F.; Jeannin, O.; Charbonnière, L. J. Molecular upconversion in water in heteropolynuclear supramolecular Tb/Yb assemblies. *J. Am. Chem. Soc.* **2019**, *141* (4), 1568−1576.
(26) Knighton, R. C.; Soro, L. K.; Lecointre, A.; Pilet, G.; Fateeva, A.; Pontille, L.; Francés-Soriano, L.; Hildebrandt, N.; Charbonniere, L. J. Upconversion in molecular hetero-nonanuclear lanthanide complexes in solution. *Chem. Commun.* **2021**, *57* (1), 53−56.
(27) Gao, C.; Zheng, P.; Liu, Q.; Han, S.; Li, D.; Luo, S.; Temple, H.; Xing, C.; Wang, J.; Wei, Y.; et al.et al. Recent advances of upconversion nanomaterials in the biological field. *Nanomaterials* **2021**, *11* (10), 2474.
(28) Magne, S.; Ouerdane, Y.; Druetta, M.; Goure, J.-P.; Ferdinand, P.; Monnom, G. Cooperative luminescence in an ytterbium-doped silica fibre. *Opt. Commun.* **1994**, *111* (3−4), 310−316.
(29) Chen, X.; Li, S.; Song, Z.; Du, W.; Wen, O.; Sawanobori, N. Study on strong cooperative upconversion luminescence of ytterbium-ytterbium clusters in oxyfluoride glass. *Josa B* **2006**, *23* (12), 2581−2587.
(30) Knighton, R. C.; Soro, L. K.; Francés-Soriano, L.; Rodríguez-Rodríguez, A.; Pilet, G.; Lenertz, M.; Platas-Iglesias, C.; Hildebrandt, N.; Charbonnière, L. J. Cooperative luminescence and cooperative sensitisation upconversion of lanthanide complexes in solution. *Angew. Chem., Int. Ed.* **2022**, *61* (4), No. e202113114.
(31) (a) Soro, L. K.; Knighton, R. C.; Avecilla, F.; Thor, W.; Przybilla, F.; Jeannin, O.; Esteban-Gomez, D.; Platas-Iglesias, C.; Charbonnière, L. J. Solution-State Cooperative Luminescence Upconversion in Molecular Ytterbium Dimers. *Adv. Opt. Mater.* **2023**, *11* (11), 2202307. (b) Kushida, T. Energy transfer and cooperative optical transitions in rare-earth doped inorganic materials. I. Transition probability calculation. *J. Phys. Soc. Jpn.* **1973**, *34* (5), 1318−1326.
(32) Haase, M.; Schäfer, H. Upconverting nanoparticles. *Angew. Chem., Int. Ed.* **2011**, *50* (26), 5808−5829.
(33) Zheng, W.; Huang, P.; Tu, D.; Ma, E.; Zhu, H.; Chen, X. Lanthanide-doped upconversion nano-bioprobes: electronic structures, optical properties, and biodetection. *Chem. Soc. Rev.* **2015**, *44* (6), 1379−1415.
(34) Gamelin, D. R.; Güdel, H. U. Design of luminescent inorganic materials: new photophysical processes studied by optical spectroscopy. *Acc. Chem. Res.* **2000**, *33* (4), 235−242.
(35) Heer, S.; Kömpe, K.; Güdel, H. U.; Haase, M. Highly efficient multicolour upconversion emission in transparent colloids of lanthanide-doped NaYF4 nanocrystals. *Adv. Mater.* **2004**, *16* (23−24), 2102−2105.
(36) Suffren, Y.; Golesorkhi, B.; Zare, D.; Guénée, L.; Nozary, H.; Eliseeva, S. V.; Petoud, S.; Hauser, A.; Piguet, C. Taming lanthanide-centered upconversion at the molecular level. *Inorg. Chem.* **2016**, *55* (20), 9964−9972.
(37) Charbonnière, L. J. Bringing upconversion down to the molecular scale. *Dalton Trans.* **2018**, *47* (26), 8566−8570.
(38) Nonat, A.; Chan, C. F.; Liu, T.; Platas-Iglesias, C.; Liu, Z.; Wong, W.-T.; Wong, W.-K.; Wong, K.-L.; Charbonnière, L. J. Room temperature molecular up conversion in solution. *Nat. Commun.* **2016**, *7* (1), 11978.
(39) Xiao, X.; Haushalter, J. P.; Faris, G. W. Upconversion from aqueous phase lanthanide chelates. *Opt. Lett.* **2005**, *30* (13), 1674−1676.
(40) Golesorkhi, B.; Nozary, H.; Guénée, L.; Fürstenberg, A.; Piguet, C. Room-Temperature Linear Light Upconversion in a Mononuclear Erbium Molecular Complex. *Angew. Chem.* **2018**, *130* (46), 15392−15396.
(41) Yin, H.-J.; Feng, Y.-S.; Liang, N.; Liu, X.-M.; Liu, J. X.; Wang, K. Z.; Yao, C.-J. Boosting Photo Upconversion in Electropolymerised Thin Film with Yb/Er Complexes. *Adv. Opt. Mater.* **2023**, *11* (6), 2202550.
(42) Wang, J.; Jiang, Y.; Liu, J. Y.; Xu, H. B.; Zhang, Y. X.; Peng, X.; Kurmoo, M.; Ng, S. W.; Zeng, M. H. Discrete heteropolynuclear Yb/Er assemblies: switching on molecular upconversion under mild conditions. *Angew. Chem.* **2021**, *133* (41), 22542−22549.
(43) Aboshyan-Sorgho, L.; Besnard, C.; Pattison, P.; Kittilstved, K. R.; Aebischer, A.; Bünzli, J. C. G.; Hauser, A.; Piguet, C. Near-Infrared→ Visible Light Upconversion in a Molecular Trinuclear d−f−d Complex. *Angew. Chem., Int. Ed.* **2011**, *50* (18), 4108−4112.
(44) Golesorkhi, B.; Taarit, I.; Bolvin, H.; Nozary, H.; Jiménez, J.-R.; Besnard, C.; Guénée, L.; Fürstenberg, A.; Piguet, C. Molecular light-upconversion: we have had a problem! When excited state absorption (ESA) overcomes energy transfer upconversion (ETU) in Cr (III)/Er (III) complexes. *Dalton Trans.* **2021**, *50* (23), 7955−7968.
(45) Knighton, R. C.; Soro, L. K.; Thor, W.; Strub, J.-M.; Cianférani, S.; Mély, Y.; Lenertz, M.; Wong, K.-L.; Platas-Iglesias, C.; Przybilla, F.; et al.et al. Upconversion in a d−f [RuYb3] Supramolecular Assembly. *J. Am. Chem. Soc.* **2022**, *144* (29), 13356−13365.
(46) Gàlico, D. A.; Calado, C. M. S.; Murugesu, M. Lanthanide molecular cluster-aggregates as the next generation of optical materials. *Chem. Sci.* **2023**, *14* (22), 5827−5841.
(47) Auzel, F.; Meichenin, D.; Pelle, F.; Goldner, P. Cooperative luminescence as a defining process for RE-ions clustering in glasses and crystals. *Opt. Mater.* **1994**, *4* (1), 35−41.
(48) Golesorkhi, B.; Fürstenberg, A.; Nozary, H.; Piguet, C. Deciphering and quantifying linear light upconversion in molecular erbium complexes. *Chem. Sci.* **2019**, *10* (28), 6876−6885.
(49) (a) Gàlico, D. A.; Murugesu, M. Controlling the Energy-Transfer Processes in a Nanosized Molecular Upconverter to Tap into Luminescence Thermometry Application. *Angew. Chem. Int. Ed.* **2022**, *61*, No. e202204839. (b) Duan, X.-F.; Zhou, L.-P.; Li, H.-R.; Hu, S.-J.; Zheng, W.; Xu, X.; Zhang, R.; Chen, X.; Guo, X.-Q.; Sun, Q.-F. Excited-Multimer Mediated Supramolecular Upconversion on Multicomponent Lanthanide-Organic Assemblies. *J. Am. Chem. Soc.* **2023**, *145* (42), 23121−23130. (c) Xu, G.; Wang, Z.-M.; He, Z.; Lü, Z.; Liao, C.-S.; Yan, C.-H. Synthesis and structural characterization of nonanuclear lanthanide complexes. *Inorg. chem.* **2002**, *41* (25), 6802−6807.
(50) Baril-Robert, F.; Petit, S.; Pilet, G.; Chastanet, G.; Reber, C.; Luneau, D. Site-selective lanthanide doping in a nonanuclear yttrium (III) cluster revealed by crystal structures and luminescence spectra. *Inorg. Chem.* **2010**, *49* (23), 10970−10976.
(51) Aguilà, D.; Roubeau, O.; Aromí, G. Designed Polynuclear Lanthanide Complexes for Quantum Information Processing. *Dalton Trans.* **2021**, *50*, 12045−12057.
(52) Marin, R.; Brunet, G.; Murugesu, M. Shining new light on multifunctional lanthanide single-molecule magnets. *Angew. Chem., Int. Ed.* **2021**, *60* (4), 1728−1746.
(53) Brunet, G.; Marin, R.; Monk, M.-J.; Resch-Genger, U.; Gàlico, D. A.; Sigoli, F. A.; Suturina, E. A.; Hemmer, E.; Murugesu, M. Exploring the dual functionality of an ytterbium complex for luminescence thermometry and slow magnetic relaxation. *Chem. Sci.* **2019**, *10* (28), 6799−6808.

(54) Kumar, K. S.; Serrano, D.; Nonat, A. M.; Heinrich, B.; Karmazin, L.; Charbonnière, L. J.; Goldner, P.; Ruben, M. Optical spin-state polarization in a binuclear europium complex towards molecule-based coherent light-spin interfaces. *Nat. Commun* **2021**, *12* (1), 2152.
(55) Pointillart, F.; Cador, O.; Le Guennic, B.; Ouahab, L. Uncommon lanthanide ions in purely 4f Single Molecule Magnets. *Coord. Chem. Rev.* **2017**, *346*, 150−175.
(56) Kishi, Y.; Cornet, L.; Pointillart, F.; Riobé, F.; Lefeuvre, B.; Cador, O.; Le Guennic, B.; Maury, O.; Fujiwara, H.; Ouahab, L. Luminescence and Single-Molecule-Magnet Behaviour in Lanthanide Coordination Complexes Involving Benzothiazole-Based Tetrathiafulvalene Ligands. *Eur. J. Inorg. Chem.* **2018**, *2018* (3−4), 458−468.
(57) Ruiz-Bilbao, E.; Pardo-Almanza, M.; Oyarzabal, I.; Artetxe, B.; Felices, L. S.; García, J. A.; Seco, J. M.; Colacio, E.; Lezama, L.; Gutiérrez-Zorrilla, J. M. Slow Magnetic Relaxation and Luminescent Properties of Mononuclear Lanthanide-Substituted Keggin-Type Polyoxotungstates with Compartmental Organic Ligands. *Inorg. Chem.* **2022**, *61* (5), 2428−2443.
(58) Errulat, D.; Marin, R.; Gàlico, D. A.; Harriman, K. L.; Pialat, A.; Gabidullin, B.; Iikawa, F.; Couto, O. D. D.; Moilanen, J. O.; Hemmer, E.; et al.etal. A luminescent thermometer exhibiting slow relaxation of the magnetization: Toward self-monitored building blocks for next-generation optomagnetic devices. *ACS Cent. Sci.* **2019**, *5*, *7*, 1187−1198.
(59) Gabarro-Riera, G.; Aromí, G.; Carolina Sañudo, E. Magnetic molecules on surfaces: SMMs and beyond. *Coord. Chem. Rev.* **2023**, *475*, 214858.
(60) Werts, M. H.; Jukes, R. T.; Verhoeven, J. W. The emission spectrum and the radiative lifetime of Eu^{3+} in luminescent lanthanide complexes. *Phys. Chem. Chem. Phys.* **2002**, *4* (9), 1542−1548.
(61) Beeby, A.; Clarkson, I. M.; Dickins, R. S.; Faulkner, S.; Parker, D.; Royle, L.; De Sousa, A. S.; Williams, J. G.; Woods, M. Non-radiative deactivation of the excited states of europium, terbium and ytterbium complexes by proximate energy-matched OH, NH and CH oscillators: an improved luminescence method for establishing solution hydration states. *J. Chem. Soc., Perkin Trans.* **1999**, *3*, 493−504.
(62) Shavaleev, N. M.; Eliseeva, S. V.; Scopelliti, R.; Bünzli, J.-C. G. Influence of symmetry on the luminescence and radiative lifetime of nine-coordinate europium complexes. *Inorg. Chem.* **2015**, *54* (18), 9166−9173.
(63) Auzel, F. A fundamental self-generated quenching center for lanthanide-doped high-purity solids. *J. Lumin.* **2002**, *100* (1−4), 125−130.
(64) Kadjane, P.; Charbonnière, L.; Camerel, F.; Lainé, P. P.; Ziessel, R. Improving visible light sensitization of luminescent europium complexes. *J. Fluoresc.* **2008**, *18*, 119−129.
(65) Chen, G.; Qiu, H.; Prasad, P. N.; Chen, X. Upconversion nanoparticles: design, nanochemistry, and applications in theranostics. *Chem. Rev.* **2014**, *114* (10), 5161−5214.
(66) Wernsdorfer, W.; Ruben, M. Synthetic Hilbert Space Engineering of Molecular Qudits: Isotopologue Chemistry. *Adv. Mater.* **2019**, *31* (26), 1806687.
(67) Sun, L.; Wei, R.; Feng, J.; Zhang, H. Tailored lanthanide-doped upconversion nanoparticles and their promising bioapplication prospects. *Coord. Chem. Rev.* **2018**, *364*, 10−32.